

Digital Control of Boost PFC Converters Operating in both Continuous and Discontinuous Conduction Mode

Koen De Gussemé*, David M. Van de Sype, Alex P. Van den Bossche, and Jan A. Melkebeek
Electrical Energy Laboratory

Department of Electrical Energy, Systems and Automation, Ghent University
Sint-Pietersnieuwstraat 41, B-9000 Gent, Belgium

*E-mail: DeGusseme@eesa.UGent.be

Abstract—Whereas power factor correction (PFC) converters for the lower power range ($< 250\text{W}$) use discontinuous conduction mode (DCM) operation, PFC converters for higher power are commonly designed for continuous conduction mode. Nevertheless, at light load, DCM will appear close to the crossover of the line voltage, causing the converter to switch between both conduction modes. As a result of this switching during a line period, the converter dynamics change abruptly, yielding input current distortion. The control scheme, presented in this paper, exploits the advantages of digital control by employing duty-ratio feedforward, in order to diminish this source of input current distortion.

I. INTRODUCTION

Power factor correction (PFC) converters for low power applications often use DC-DC converters such as buck-boost, boost, SEPIC or Čuk converters, operated in discontinuous conduction mode (DCM). After all, these converters require only a single control loop [1]–[3] to assure both a resistive input and a constant output voltage. Nevertheless, due to high device stresses and problems with conducted emission, the use of converters operating in DCM is limited to the low power range ($< 250\text{W}$).

Therefore, many power factor correction converters for the higher power range are operated in the continuous conduction mode (CCM). One of the most popular topologies is that of the boost PFC converter, see Fig. 1. Since a lot of research on the control of these converters has been performed [10]–[16], input current waveforms with very low harmonic distortion can be achieved, as long as a continuous inductor current is assured. Nevertheless, when these converters are operated at light load, DCM will appear close to the crossover of the line voltage [4]–[7], causing the converter to switch between CCM and DCM (this mode of operation will be referred to as mixed conduction mode or MCM). As a result of this switching during a line period, the converter dynamics change abruptly [3]–[9], yielding input current distortion. Moreover, when the load is further decreased, the converter will operate in DCM during the entire line period. Since the input current controller is designed for operation in CCM, and the corresponding system transfer functions in CCM and DCM differ, the input current tracking will not be satisfying.

To avoid these problems, a large input inductor L can be chosen, depending on the expected minimum of the power. Another possibility [7] is to change the switching frequency and the controller when the load is approaching critical conduction mode. This way, the converter is operated in DCM for low input power, with a controller adapted to DCM operation, while for high power, CCM operation is maintained.

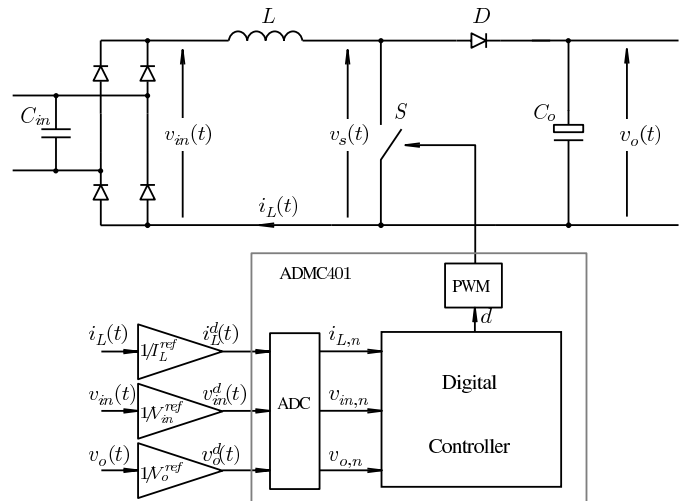


Fig. 1. A digitally controlled boost PFC converter

Nevertheless, a converter with a low value of the input inductor L , and a fixed switching frequency is still desirable to reduce the weight and to allow an easier design of the EMI-filter. Therefore, it is necessary that the control algorithm is able to deal with sudden changes in converter dynamics. Such a control algorithm is described in this paper. The proposed control scheme exploits the advantages of digital control by employing duty-ratio feedforward, a technique previously applied with success for PFC converters operating solely in CCM [16]. After the introduction of this control algorithm, its influence on the input impedance of a boost PFC converter is calculated in detail. All theoretical results are verified using an experimental 1kW boost PFC converter.

II. DIGITAL CONTROL OF A BOOST PFC CONVERTER WITH PI-CONTROLLERS

A. Typical digital control of the boost PFC converter

Just like its analog equivalent, a typical digital controller for a boost PFC converter is composed of two control loops, one to control the output voltage, and one to control the input current. The reference value for the output voltage controller is an external input, while the reference input current is obtained by multiplying the input voltage with the desired input conductance of the converter, which is supplied by the output voltage controller. This controller is depicted in Fig. 2. Since a digital controller performs its control actions on the digital quantities $i_{L,n}$, $v_{in,n}$, and $v_{o,n}$, an analog-to-digital conversion is required. Mathematically, this can be represented

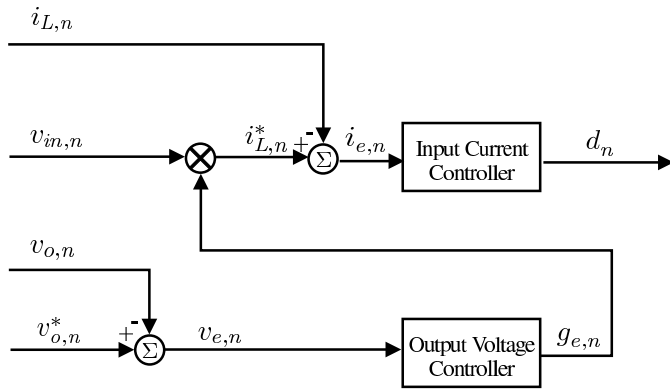


Fig. 2. A typical controller for a boost PFC converter

as a division of the control values, the inductor current $i_L(t)$, the input voltage $v_{in}(t)$ and the output capacitor voltage $v_o(t)$ by their reference values I_L^{ref} , V_{in}^{ref} and V_o^{ref} , and a sampling process using an analog-to-digital converter (ADC). Nevertheless, for the remainder of this paper the absolute values of the control variables are used, in order to reduce the complexity of the calculations. However, all results and conclusions remain unaltered.

The sampling rate of this process is commonly chosen equal to the switching frequency. As a result of this synchronization between the switching and the sampling, all control variables are represented by one sample each switching cycle. Since the input and output voltage are varying slowly, the exact sampling instant does hardly affect the values of the input and output voltage samples. To obtain a good representation of the input current, it is important that the sampling instant is chosen in the middle of the rising edge of the input current waveform [14]. This way, the average input current $\langle i_L \rangle$ is obtained in CCM. In order to obtain the correct value of this input current sample in the DCM part of the line period, the sample must be multiplied by a factor κ , as defined in [5].

B. The input current response in CCM and DCM

For operation in CCM, the input current response to small variations \hat{d} , \hat{v}_{in} , and \hat{v}_o on the steady-state duty-ratio D , input voltage V_{in} , and output voltage V_o are calculated in [13] and [16]

$$\hat{v}_L(s) = \frac{1}{sL} \hat{v}_{in}(s) + \frac{V_o}{sL} \hat{d}(s) - \frac{1-D}{sL} \hat{v}_o(s) \quad (1)$$

leading to the transfer function of the system to be controlled, the duty-ratio-to-input-current transfer function

$$G_i^{ccm}(s) = \frac{\hat{v}_L(s)}{\hat{d}(s)} = \frac{V_o}{sL}, \quad (2)$$

This transfer function is depicted in Fig. 3, gray trace, with the parameters of the experimental converter (see section V).

When the converter is operated in DCM, the system dynamics change drastically. The corresponding averaged converter model is obtained by applying the averaging method of [8], yielding

$$\frac{d\langle i_L \rangle}{dt} = \frac{2\langle i_L \rangle}{dT} \left(1 - \frac{v_o}{v_{in}} \right) + \frac{dv_o}{L}. \quad (3)$$

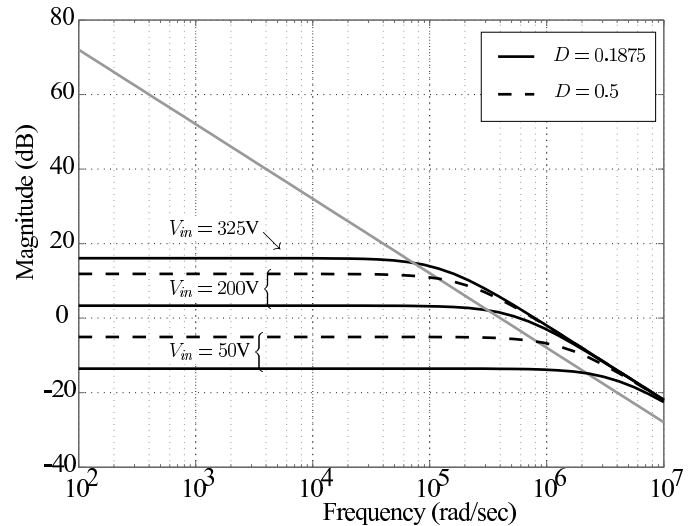


Fig. 3. Duty-ratio-to-input-current transfer function for ccm (gray trace) and dcm (black traces)

From (3), the steady-state equation can be calculated

$$\langle I_L \rangle = \frac{D^2 T V_{in} V_o}{2L (V_o - V_{in})}. \quad (4)$$

Using standard linearization techniques and the Laplace transform, the input current response to small variations of the duty-ratio, the input voltage and the output voltage can be obtained

$$\hat{v}_L(s) \left\{ s + \frac{2(V_o - V_{in})}{DTV_{in}} \right\} = \frac{2V_o}{L} \hat{d}(s) + \frac{DV_o^2}{L(V_o - V_{in})V_{in}} \hat{v}_{in}(s) - \frac{DV_{in}}{L(V_o - V_{in})} \hat{v}_o(s), \quad (5)$$

leading to the duty-ratio-to-inductor-current transfer function

$$G_i^{dcm}(s) = \frac{\hat{v}_L(s)}{\hat{d}(s)} = \frac{\frac{2V_o}{L}}{s + \frac{2(V_o - V_{in})}{DTV_{in}}}. \quad (6)$$

Fig. 3 shows the amplitude of the obtained transfer function (6) under different conditions of the steady-state duty-ratio D and input voltage V_{in} and for a constant output voltage V_o . For the parameters of the experimental converter of section V, the low frequency gain of this transfer function reaches its maximum value for $V_{in} = 325V$ and $D = 0.1875$, corresponding with the upper black curve in Fig. 3.

In most cases, the frequency corresponding to the pole of $G_i^{dcm}(s)$ is higher than the switching frequency (50kHz in our case) and certainly much higher than the cut-off frequency of the current control loop. Consequently, the open loop gain in DCM will be much lower than in CCM. This will cause poor inductor current tracking and important input current distortion if the same controller as in CCM is employed in DCM.

C. PI-controllers with variable parameters

Since the transfer function of the system is different in CCM and DCM, an obvious choice would be to detect the conduction mode and change the control parameters when switching from one conduction mode to another. For operation

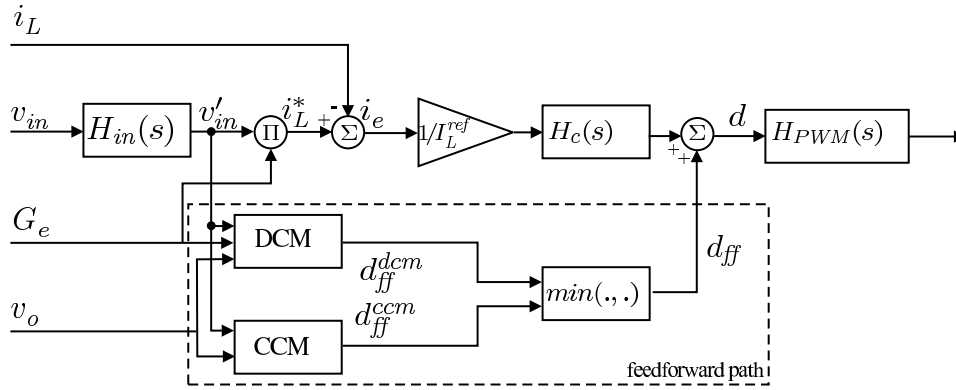


Fig. 4. The current loop controller with duty-ratio feedforward

in either CCM or DCM, this approach guarantees low input current distortion. Nevertheless, in MCM some problems arise: detection of the conduction mode is difficult as the sensing and sampling of the appropriate variables (the inductor current or the input and output voltages...) may introduce some errors, and the border between continuous and discontinuous conduction mode is crossed slowly (it may take several switching cycles). This may cause the DCM controller to be active during CCM operation or vice versa. Since the gain of the DCM-controller should be much higher than the gain of the CCM-controller, the system will become unstable in the first case, while in the case of a CCM-controller in the DCM-part of the line period will cause poor tracking. Hence, the resulting input current waveform will still be distorted.

III. DUTY-RATIO FEEDFORWARD

In [16], feedforward of the duty-ratio in CCM has been proposed. In this control algorithm, see Fig. 4, the ideal value of the duty-ratio is calculated and added to the output of the controller, which is the unaffected PI-controller used in CCM. One of the features of this control algorithm is the excellent input current waveform, even for low gain of the controller H_c . A similar control algorithm would be suitable for the control of this converter in MCM, where the gain of the duty-ratio-to-inductor-current transfer function in DCM depends on the steady-state duty-ratio and input voltage, and is different from CCM. In CCM, the value of the forwarded duty-ratio d_{ff}^{ccm} can be derived from an expression of the ideal switch voltage [16], yielding

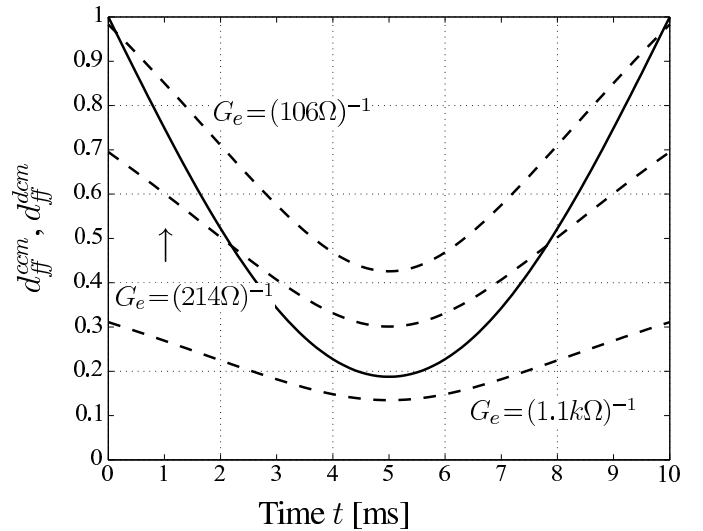
$$d_{ff}^{ccm} = 1 - \frac{v_{in}}{v_o}. \quad (7)$$

For operation in DCM, equation (4) reveals that the input current is directly related to the duty-ratio. Therefore, the duty-ratio assuring an ideal input current waveform $i_L(t) = G_e v_{in}(t)$ can be calculated

$$d_{ff}^{dcm} = \sqrt{\frac{2G_e L}{T} \cdot \frac{v_o - v_{in}}{v_o}}, \quad (8)$$

with G_e the desired input conductance of the converter. Both (7) and (8) are displayed in Fig. 5, the solid line and the dashed lines respectively. The intersection of both curves can be calculated as

$$d = \frac{2G_e L}{T}, \quad (9)$$


 Fig. 5. Ideal values of the duty-ratio d_n for operation in CCM (solid line), or DCM (dashed line)

which corresponds with operation in the critical conduction mode [5]. Hence, the required duty-ratio for operation in the mixed conduction mode, is a combination of the DCM and the CCM curve, and the correct value for d_{ff} is obtained by taking the lowest value of the two duty-ratios d_{ff}^{ccm} and d_{ff}^{dcm} . As a result, the take over between the two conduction modes will not cause a jump in the forwarded duty-ratio. When feedforward is used, the controller is compensating only for low values of the input current error. Therefore, the PI-controller designed for the control of the converter in CCM can be maintained during the entire operation in MCM, yielding low input current distortion near the take over between CCM and DCM. A schematic representation of the input current controller, including duty-ratio feedforward, is shown in Fig. 4.

IV. THE SMALL-SIGNAL INPUT IMPEDANCE OF THE CONVERTER

A. Calculation of the impedance

The input impedance of the converter in the continuous conduction mode, with and without duty-ratio feedforward,

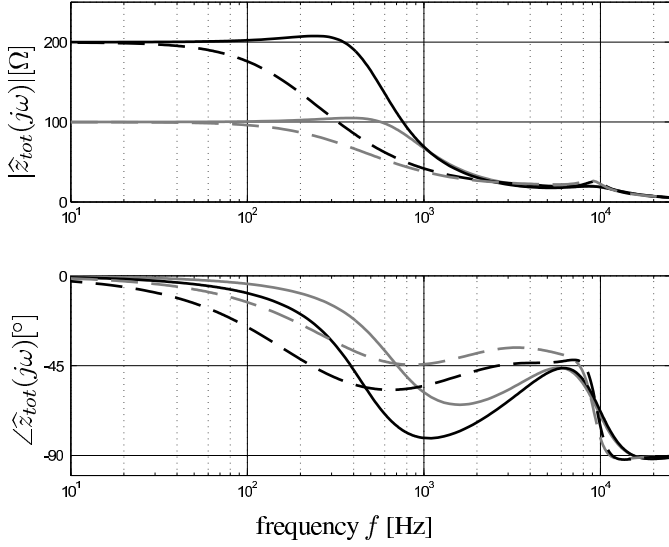


Fig. 6. The total small-signal input impedance of the boost PFC converter in CCM; dashed lines: without feedforward, full lines: with feedforward; black lines $G_e = (200\Omega)^{-1}$, $V_{in} = 230V$, gray lines: $G_e = (100\Omega)^{-1}$, $V_{in} = 230V$

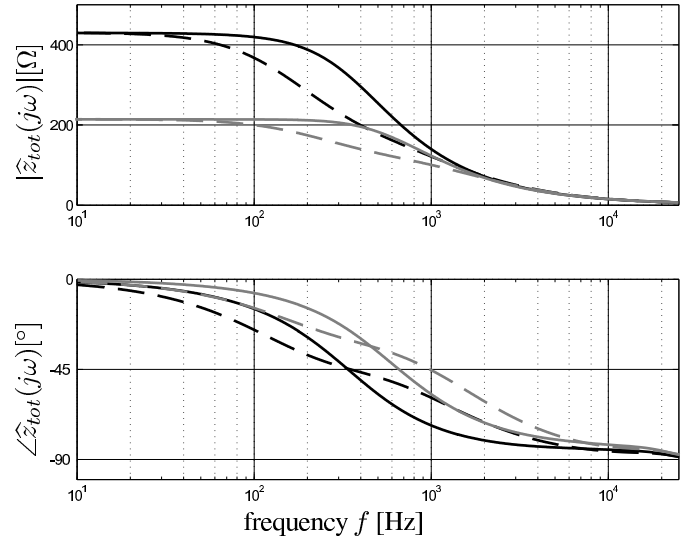


Fig. 7. The total small-signal input impedance of the boost PFC converter in DCM; dashed lines: without feedforward, full lines: with feedforward; black lines $G_e = (430\Omega)^{-1}$, $V_{in} = 230V$, gray lines: $G_e = (214\Omega)^{-1}$, $V_{in} = 180V$

is calculated in [16], yielding

$$\hat{z}_{in}(s) = \frac{\hat{v}_{in}(s)}{\hat{i}_L(s)} = \frac{sL + \frac{V_o}{I_L^{ref}} H_c(s) H_{PWM}(s)}{(1 - KH_{in}(s)H_{PWM}(s)) + \frac{V_o G_e}{I_L^{ref}} H_c(s) H_{in}(s) H_{PWM}(s)}, \quad (10)$$

where $K = 0$ when considering operation without duty-ratio feedforward, and $K = 1$ when operation with duty-ratio feedforward is considered.

For the calculation of the input impedance of the converter in the discontinuous conduction mode, a linearization is required, since the duty-ratio feedforward using (8) introduces non-linearities in the input current control loop. Using capitals for steady-state values, and hatted small letters for small excursions from steady-state, the linearized version of the non-linear feedforward path becomes

$$\hat{d}_{ff} = \frac{\hat{v}_o}{V_o} \left(\frac{G_e L}{DT} - \frac{D}{2} \right) - \frac{\hat{v}'_{in}}{V_o} \frac{G_e L}{DT}. \quad (11)$$

Taking into account that $V'_{in} \approx V_{in}$ and $\hat{v}'_{in}(s) = H_{in}(s)\hat{v}_{in}(s)$, allows to derive the small-signal transfer function of the current loop controller (Fig. 4)

$$\hat{d} = H_{PWM}(s)H_{in}(s) \left(\frac{H_c(s)G_e}{I_L^{ref}} - K \frac{G_e L}{DTV_o} \right) \hat{v}_{in} - \frac{H_{PWM}(s)H_c(s)}{I_L^{ref}} \hat{v}_L(s) + K \frac{H_{PWM}(s)}{V_o} \left(\frac{G_e L}{DT} - \frac{D}{2} \right) \hat{v}_o. \quad (12)$$

By eliminating the duty-ratio \hat{d} in (5) and (12), the input

current of the converter becomes

$$\hat{i}(s) \left\{ s + \frac{2D}{2G_e L - D^2 T} + H_c(s)H_{PWM}(s) \frac{2V_o}{LI_L^{ref}} \right\} = \hat{v}_o(s) \left\{ KH_{PWM}(s) \frac{2}{L} \left(\frac{G_e L}{DT} - \frac{D}{2} \right) - \frac{2G_e}{DT} \left(1 - \frac{D^2 T}{2G_e L} \right) \right\} + \hat{v}_{in}(s) \left\{ \frac{4G_e^2 L}{DT(2G_e L - D^2 T)} + 2G_e H_{PWM}(s)H_{in}(s) \left(\frac{V_o}{LI_L^{ref}} H_c(s) - \frac{K}{DT} \right) \right\}. \quad (13)$$

Hence, the small-signal input impedance of the converter is

$$\hat{z}_{in}(s) = \frac{\hat{v}_{in}(s)}{\hat{i}_L(s)} = \frac{\frac{1}{G_e} \left(s + \frac{2D}{2G_e L - D^2 T} + H_c(s)H_{PWM}(s) \frac{2V_o}{LI_L^{ref}} \right)}{2H_{PWM}(s)H_{in}(s) \left(\frac{V_o}{LI_L^{ref}} H_c(s) - \frac{K}{DT} \right) + \frac{4G_e^2 L}{DT(2G_e L - D^2 T)}}. \quad (14)$$

In this input impedance, the influence of the grid impedance is not taken into account. Neglecting the grid impedance is only allowed when a filter capacitance is inserted between the grid and the diode bridge of the converter. The capacitance of this filter capacitor should be chosen in such a way that the impedance of this capacitor at the switching frequency is much lower than the impedance of the grid. In this case, the unknown grid impedance can be neglected, but the impedance of the input capacitor has to be taken into account. Therefore, the total input impedance of the converter becomes

$$\hat{z}_{tot}(s) = (\hat{z}_{in}^{-1}(s) + sC_{in})^{-1}. \quad (15)$$

B. The different transfer functions for a digitally controlled boost PFC converter

To obtain quantitative results for the input impedances (10) and (14), the transfer functions of some additional blocks of

the control scheme of Fig. 4 are required. These are:

- A low-pass filter in the signal chain of the input voltage. This filter is required to ensure the stability of the converter [12]. An analog first-order filter was inserted

$$H_{in}(s) = \frac{1}{1 + s\tau_f}. \quad (16)$$

- The transfer function of the input current controller. Although this controller is implemented digitally, the transfer function of its continuous equivalent is used with good accuracy

$$H_c(s) = K_{PI} \left(1 + \frac{1}{s\tau_{PI}} \right). \quad (17)$$

Since this transfer function is dimensionless, a division by I_L^{ref} must be inserted in the signal chain.

- the transfer function of the PWM modulator [17]

$$H_{PWM}(j\omega) = \cos\left(\frac{\omega DT}{2}\right) e^{-j\frac{\omega T}{2}} \cdot e^{-j\frac{\omega T}{2}}, \quad (18)$$

where one delay of half a switching period is due to the modulator, and another delay is due to the time required for the calculations of the processor.

C. Discussion of the results

Figs. 6 and 7 display the amplitude and the angle of the small-signal input impedance of the converter, calculated with (10) and (15) for the continuous conduction mode operation (Fig. 6, [16]), and with (14) and (15) for the discontinuous conduction mode (Fig. 7). The full lines correspond with $K = 1$ and represent the impedance when duty-ratio feedforward is applied, while the dashed lines represent the impedance of the converter controlled by a PI-controller, corresponding with $K = 0$. The curves are obtained using the values of the experimental verification described in V.

Fig. 6 shows that, whereas for operation without duty-ratio feedforward, the amplitude of the input impedance starts setting already at low frequencies, a constant impedance of the converter up to a frequency of 1kHz or higher is achieved when duty-ratio feedforward is inserted in the control loop. This frequency decreases when G_e is increased, due to the higher importance of the input capacitor of the converter. This capacitor causes the converter to behave more and more capacitive when G_e is increased (corresponding with a decrease of the load). Therefore, even at low frequencies, a small phase displacement between the input current and the input voltage will exist.

The same trends are observed in Fig. 7, displaying the input impedance in the discontinuous conduction mode: since operation in DCM occurs at low power levels, or high values of the desired input conductance G_e , the influence of the input capacitance becomes more important, and the behavior of the converter will approach very close the behavior of a capacitor in parallel with a resistor with value $\frac{1}{G_e}$. This is demonstrated theoretically by assuming $\tau_{PI} \gg \tau_f$ and $\tau_{PI} \gg T$, and for angular frequencies lower than $\frac{1}{\tau_{PI}}$, where

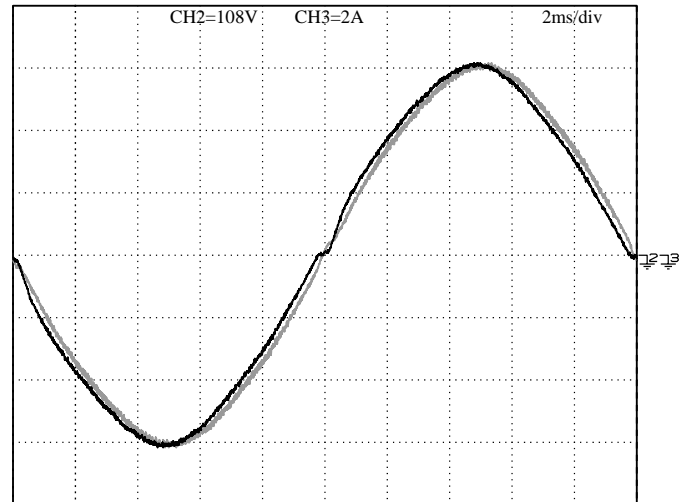


Fig. 8. Input current and input voltage waveforms at full load (1kW), in CCM operation

the input conductance (14) for DCM becomes

$$\hat{z}_{in} \approx \frac{1}{G_e} \cdot \frac{j\omega \left(\alpha\tau_{PI} + \frac{2DL}{2G_e L - D^2 T} \right) + \alpha}{j\omega \left(\alpha\tau_{PI} + \frac{4G_e L^2}{DT(2G_e L - D^2 T)} - K \frac{2L}{DT} \right) + \alpha}, \quad (19)$$

with

$$\alpha = \frac{V_o K_{PI}}{I_L^{ref} \tau_{PI}}. \quad (20)$$

For operation with duty-ratio feedforward ($K = 1$), the numerator of (19) equals the denominator, and the input impedance becomes $\hat{z}_{in} = \frac{1}{G_e}$.

V. EXPERIMENTAL RESULTS

In order to verify the analysis and to test the proposed control algorithm, a 1kW boost PFC converter was built with the following converter parameters

$$\begin{cases} V_g = 230V, & f_g = 50Hz, & T = 19.6\mu s \\ V_o = 400V, & C_o = 470\mu F, & L = 1mH \end{cases} \quad (21)$$

The power range for this converter to operate in the mixed conduction mode, is calculated in [5], yielding a zone between 100W and 500W.

The input current waveforms of this converter at different power levels are displayed in Figs. 8–10. Operation at full power is shown in Fig. 8, with its typical two-loop controller and feedforward in CCM. Measurement of the total harmonic distortion, and the power factor reveal the very good performance of this control configuration in CCM: the THD is lower than 2%, while the power factor is near unity.

For operation at 125W and 70W programmed input power, yielding MCM and DCM operation respectively, the waveforms are shown in Figs. 9–10 for two different controllers: operation with the PI-controller for CCM operation (Fig. 9), and operation with duty-ratio feedforward (Fig. 10). Whereas in Fig. 9 the difference in dynamics between DCM and CCM causes a disturbance in the input current at the crossover between CCM and DCM, and causes poor input current tracking in the DCM-part of the line period, the input current

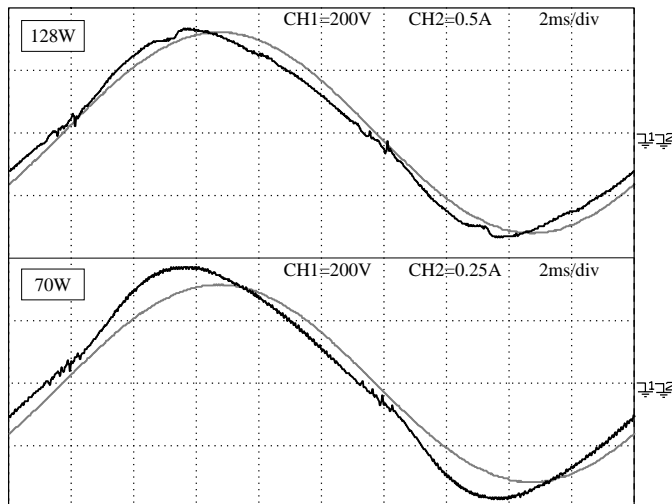


Fig. 9. Input current and input voltage waveforms for 128 and 70W programmed input power, without feedforward

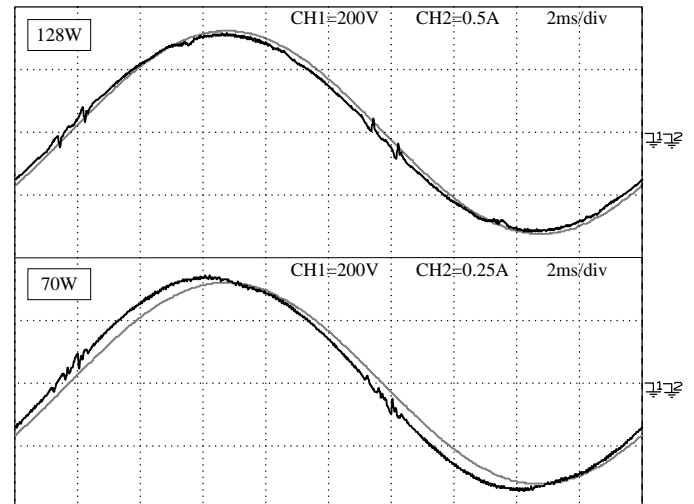


Fig. 10. Input current and input voltage waveforms for 128 and 70W programmed input power, with duty-ratio feedforward

TABLE I

EXPERIMENTAL MEASUREMENTS OF THE THD AND THE POWER FACTOR, PI=PI-CONTROLLER, AND FF= FEEDFORWARD

P_{in}^p [W] $= G_e V_g^2$	THD [%]		power factor	
	PI	FF	PI	FF
252	6.5	2.4	0.993	0.999
128	7.2	2.8	0.988	0.997
70	9.1	2.8	0.976	0.992

waveforms in Fig. 10 are very close to the input voltage waveform for both values of the input power. Note that for low values of the desired input conductance G_e , the influence of the filter capacitance of the EMI-filter becomes important, causing a small displacement between the input current and the input voltage.

In order to quantify the improvements achieved by the new control algorithm, the total harmonic distortion (THD), and the power factor are measured for three values of the input power, 252W, 128W (MCM), and 70W (DCM). The results are shown in Table. I. For all cases, an important decrease of the total harmonic distortion is observed. Moreover, the power factor becomes higher than 0.99 when duty-ratio feedforward is applied, and is limited by the input capacitance of the converter.

For the verification of the theoretical input impedance of the converter, calculated in section IV, the experimental setup was supplied by a linear power source, supplying a small sine wave superposed on a DC voltage. The input impedance was obtained experimentally for two values of the input power, 250W (Fig. 11), and 125W (Fig. 12), corresponding with $G_e = (214\Omega)^{-1}$ and $G_e = (430\Omega)^{-1}$ respectively. Nevertheless, since the converter operates in the continuous conduction mode when $G_e = (214\Omega)^{-1}$ and $V_{in} = 230V$, the input voltage was decreased from 230V to 180V for this measurement, thus yielding operation in the discontinuous conduction mode, but close to the critical conduction mode. For both

$G_e = (214\Omega)^{-1}$ and $G_e = (430\Omega)^{-1}$, the experimental results match the theoretical curves very well, so the validity of the theoretical analysis is confirmed. For 70W input power no results are shown because for the corresponding value of the desired input conductance G_e , the input impedance is mainly determined by the input capacitor.

VI. CONCLUSIONS

Power factor correction converters for applications at a power higher than 250W, are commonly operated in the continuous conduction mode. Nevertheless, when these converters are operated at light load, operation in the discontinuous conduction mode appears during parts of the grid period, yielding operation in the mixed conduction mode. Since the converter dynamics are different in CCM and DCM, operation in MCM will cause input current distortion. Therefore, the control algorithm is extended with duty-ratio feedforward, resulting in input current waveforms which are very close to the input voltage waveforms. In the theoretical analysis of this control algorithm, the input impedance of the converter was calculated, confirming the very good resistive behavior of the converter when duty-ratio feedforward is employed. Experimental results using a 1kW boost PFC converter, confirm both the correctness of the theoretical analysis, as well as the improvements on the input current waveform and the reduction of the input current harmonics achieved with this control algorithm.

REFERENCES

- [1] J. Sebastian, J.A. Martínez, J.M. Alonso, and J.A. Cobos, "Voltage-follower control in zero-current-switched quasi-resonant power factor preregulators," *IEEE Trans. Power Electr.*, Vol. 13, No. 4, July 1998, pp. 727-738.
- [2] D.S.L. Simonetti, J. Sebastian, and J. Uceda, "The discontinuous conduction mode sepic and cuk power factor preregulators: analysis and design," *IEEE Trans. Ind. Electr.*, Vol. 44, No. 5, Oct. 1997, pp. 630-637.
- [3] D.S.L. Simonetti, J.L.F. Vieira, and G.C.D. Sousa, "Modeling of the high-power-factor discontinuous boost rectifiers," *IEEE Trans. Ind. Electr.*, Vol. 46, No. 4, Aug. 1999, pp. 788-795.

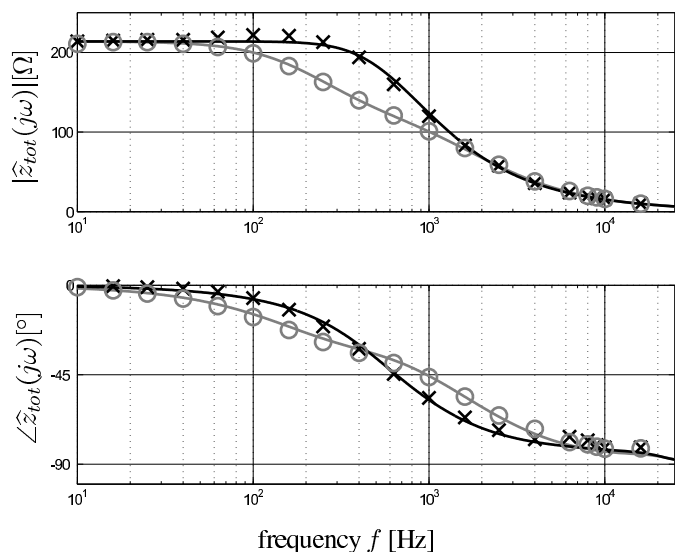


Fig. 11. Experimental results (markers) versus theory (full lines) for the total input impedance \hat{z}_{tot} with $G_e = (214\Omega)^{-1}$ and $V_{in} = 180V$, black lines: with feedforward, gray lines: without feedforward

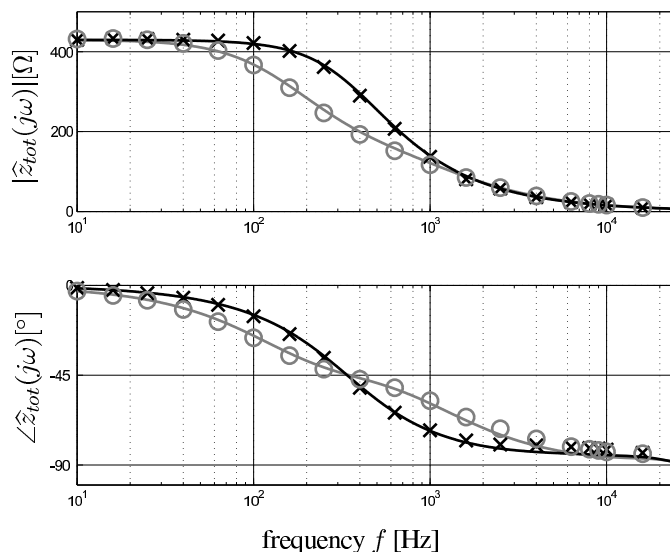


Fig. 12. Experimental results (markers) versus theory (full lines) for the total input impedance \hat{z}_{tot} with $G_e = (430\Omega)^{-1}$ and $V_{in} = 230V$, black lines: with feedforward, gray lines: without feedforward

[4] J. Sebastian, J.A. Cobos, J.M. Lopera, and J. Uceda, "The determination of the boundaries between continuous and discontinuous conduction modes in pwm dc-to-dc converters used as power factor preregulators," *IEEE Trans. Power Electr.*, Vol. 10, No. 5, Sept. 1995, pp. 574–582.

[5] K. De Gussemé, D.M. Van de Sype, A.P. Van den Bossche, and J.A. Melkebeek, "Sample correction for digitally controlled boost pfc converters operating in both ccm and dcm," *Proc. of the IEEE Appl. Power Electr. Conf.*, APEC 2003, Feb. 9–13, 2003, Miami Beach, Florida, USA, pp. 389–395.

[6] K. De Gussemé, D.M. Van de Sype, A.P. Van den Bossche, and J.A. Melkebeek, "Input current distortion of ccm boost pfc converters operated in dcm," *Proc. of the IEEE Power Electr. Spec. Conf.*, PESC 2003, June 15–19, 2003, Acapulco, Mexico, pp. 1685–1690.

[7] R.K. Tripathi, S.P. Das, and G.K. Dubey, "Mixed-mode operation of boost switch-mode rectifier for wide range of load variations," *IEEE Trans. Power Electr.*, Vol. 17, No. 6, Nov. 2002, pp. 999–1009.

[8] J. Sun, D.M. Mitchell, M.F. Greuel, P.T. Krein, and R.M. Bass, "Averaged modeling of pwm converters operating in discontinuous conduction mode," *IEEE Trans. Power Electr.*, Vol. 16, No. 4, July 2001, pp. 482–492.

[9] V. Vorpérian, "Simplified analysis of pwm converters using model of pwm switch, part II: discontinuous conduction mode" *IEEE Trans. Aero. Electr. Sys.*, Vol. 26, No. 3, May 1990, pp. 497-505.

[10] S. Buso, P. Mattavelli, L. Rossetto, and G. Spiazzi, "Simple digital control improving dynamic performance of power factor preregulators," *IEEE Trans. Power Electr.*, Vol. 13, No. 5, Sept. 1998, pp. 814–823.

[11] A.H. Mitwalli, S.B. Leeb, G.C. Verghese, and V.J. Thottuvellil, "An adaptive digital controller for a unity power factor converter," *IEEE Trans. Power Electr.*, Vol. 11, No. 2, March 1996, pp. 374–382.

[12] G. Spiazzi, and J.A. Pomilio, "Interaction between EMI filter and power factor preregulators with average current control: analysis and design considerations," *IEEE Trans. Ind. Electr.*, Vol. 46, No. 3, June 1999, pp. 577–584.

[13] K. De Gussemé, D.M. Van de Sype, and J.A.A. Melkebeek, "Design issues for digital control of boost power factor correction converters," *Proc. of the IEEE Int. Symp. Ind. Electr.*, ISIE 2002, July 8–11, 2002, L'Aquila, Italy, pp. 731–736.

[14] D.M. Van de Sype, K. De Gussemé, and J.A.A. Melkebeek, "A sampling algorithm for digitally controlled boost PFC converters," *IEEE Trans. Power Electr.*, in press.

[15] S. Sivakumar, K. Natarajan, and R. Gudelewicz, "Control of power factor controlling boost converter without instantaneous measurement of input current," *IEEE Trans. Power Electr.*, Vol. 10, No. 4, July 1995, pp. 435–445.

[16] D.M. Van de Sype, K. De Gussemé, A.P. Van den Bossche, and J.A. Melkebeek, "Duty-ratio feedforward for digitally controlled boost pfc converters," *Proc. of the IEEE Appl. Power Electr. Conf.*, APEC 2003, Feb. 9–13, 2003, Miami Beach, Florida, USA, pp. 396–402

[17] D.M. Van de Sype, K. De Gussemé, A.P. Van den Bossche, and J.A. Melkebeek, "Small-Signal Laplace-Domain Analysis of Uniformly-Sampled Pulse-Width Modulators," *Proc. of the IEEE Power Electr. Spec. Conf.*, PESC 2004, June 20–25, 2004, Aachen, Germany, on CD-rom.